Mitigating Reflection Cracking in Asphalt Concrete Overlays with ECC and Geotextile

Amjad H. Albayati
Department of Civil Engineering, University of Baghdad, Iraq
a.khalil@uobaghdad.edu.iq (corresponding author)

Nazar K. Oukaili
Department of Civil Engineering, University of Baghdad, Iraq
nazar.oukaili@coeng.uobaghdad.edu.iq

Hadel Obaidi
Department of Water Resources Techniques, Institute of Technology, Iraq | Middle Technical University, Iraq
hadel.obaidi@gmail.com

Bahaa M. Alatta
Department of Civil Engineering, University of Baghdad, Iraq
balatta@coeng.uobaghdad.edu.iq

Received: 21 November 2023 | Revised: 1 December 2023 and 16 December 2023 | Accepted: 18 December 2023

 DOI: https://doi.org/10.48084/etasr.6650

ABSTRACT

The rehabilitation of deteriorated pavements using Asphalt Concrete (AC) overlays consistently confronts the reflection cracking challenge, where inherent cracks and joints from an existing pavement layer are mirrored in the new overlay. To address this issue, the current study evaluates the effectiveness of Engineered Cementitious Composite (ECC) and geotextile fabric as mitigation strategies. ECC, characterized by its tensile ductility, fracture resistance, and high deformation capacity, was examined in interlayer thicknesses of 7, 12, and 17 mm. Additionally, the impact of geotextile fabric positioning at the base and at 1/3 depth of the AC specimen was explored. Utilizing the Overlay Testing Machine (OTM) for evaluations, the research demonstrated that ECC17 significantly mitigated reflection cracking, showing a notable 764% increase in the number of load cycles to failure (Nf) compared to the Geotextile Base (GB) specimen. Against the Reference Specimen (RS), ECC17 exhibited a remarkable 1307% enhancement in Nf values, underscoring its effectiveness. Geotextile fabric, particularly at 1/3 depth, demonstrated notable resistance but was overshadowed by the performance of ECC interlayers. The results clearly indicate that ECC, especially ECC17, stands out as an effective solution for mitigating reflection cracking, including joints, in AC overlays.

Keywords-reflection cracking; asphalt concrete overlay; geotextile; engineered cementitious composite; overlay testing machine

I. INTRODUCTION

Applying Asphalt Concrete (AC) overlays is the most commonly used method for rehabilitating deteriorated pavements. However, they do not often perform as satisfactorily as expected because of the existing cracks that propagate through the newly constructed overlay within a short period of time (reflection cracking). This phenomenon is widespread and is considered one of the most dominant existing pavement problems [1, 2]. Reflection cracking is caused by one or more cycles of thermal contraction, repeated traffic loads, or by a combination of both. Cracks in old pavements frequently spread to the surface within one to five years if the new overlay is bonded to the damaged layer [3, 4]. Reflection cracks significantly shorten the road lifespan and make its maintenance more complex and expensive. This results in water entering the pavement structure, contributing to pavement deterioration forms, namely increased roughness, spalling, and decreased fatigue life [5]. Existing design methods do not generally provide criteria to mitigate reflection cracking. Aiming to minimize or delay this problem occurrence, techniques such as overlay thickness increase, modification of the asphalt properties, and placement of stress-

relieving interlayers have been attempted, showing, though, limited success [6].

Numerous strategies have been used to control the growth of reflection cracks as a result of the problem's aggravation. Some of these techniques, such as increasing the thickness of the overlay, modification of asphalt properties, and placement of stress-relieving interlayers, have successfully decreased reflective cracking in particular situations, but the degree of success is usually limited. Other methods employed to alleviate reflective cracking complications, include saw and seal, fractured slabs, and many forms of interlayers. Table I provides a summary of the treatment methods discussed in the literature, along with ways to prevent reflective cracking.

TABLE I. SUMMARY OF TREATMENT METHODS FOR MITIGATING REFLECTIVE CRACKING

Treatment Method	Advantages	Disadvantages
Increasing the thickness of the asphalt overlay [8-9]	When using comparable asphalt materials, thicker overlays perform better than thinner ones.	This is not a cost-effective approach because more overlays require more material
Crack and seat [10-11]	This is economical and appropriate for asphalt surfaces with cracks	Reflection cracking could be still occurred.
Rubblisation [12-13]	Rubblisation reduces the possibility of moving underneath the asphalt overlay, thus providing a successful strategy for delaying reflective cracking.	It isn't recommended to overlay the existing concrete pavements containing steel reinforcement.
Strain Alleviating Membranes Interlayer (SAMI) [14]	This method is considered the solution to prevent reflective cracking for up to five years	It cannot prevent reflective cracking when significant traffic loads (such as aircraft) are anticipated.
Application of asphalt geosynthetics within or underneath asphalt layers [15-16]	It is considered an efficient technique	Uncertainties exist regarding the best location for installing the geosynthetic layers for the best results.
Crack relieving interlayers [17]	This technique can be classified as a solution of short-term	The reflective cracks cannot be removed by it. It suggests combining this method with other immediate solutions for a better result.

The majority of the methods illustrated above are either ineffective or only extend the pavement overlay service by a few years. The treatment process commonly used to control reflection fractures has been extensively studied through lab tests [18], finite element simulations [19], and test road constructions [20]. These findings demonstrate that despite the semi-rigid base material high strength, the pavement is easily deformed and contracts with changes in humidity and temperature, leading to transverse contraction cracks [21]. One of the newly proposed techniques is using bendable concrete or Engineered Cementitious Composites (ECCs), placed between the existing pavement and the actual overlay. Commonly, ECC is composed of protland cementy type 1, low calcium Class-F fly ash, or other pozzlanic materials. It may also encompass fine silica sand, Polyvinyl Alcohol (PVA) fibers, or other high tensile strength fibers, water, and superplasticizer. The PVA can make the concrete more flexible, and thus bendable [22-24]. Bendable concrete utilization provides several advantages compared to conventional concrete, including increased flexibility, reduced weight (by 20 to 40%), and increased crack resistance. Additionally, this concrete type has the ability to heal itself and does not emit the hazardous gases that are created when manufacturing conventional concrete. However, similarly to the other methods employed to mitigate reflective cracking, bendable concrete entails certain drawbacks. It has a higher beginning cost than conventional concrete, despite the fact that it can lower the overall project cost. Moreover, skilled labor is necessary for its construction while ECC quality is influenced by the materials utilized and the present environmental conditions [24, 25].

Several studies suggest additional ways to control the reflected cracking problem. For instance, geotextiles have rather strong mechanical properties, are resistant to bio-degradation, and offer cost-effective solutions for applications in civil engineering [26]. Geotextiles require less skill to install and are more affordable than conventional materials, such as concrete and gravel [27]. Additionally, by avoiding the intermixing of the base layer and subgrade particles, geotextiles can improve pavement performance while saving time and cost by reducing the requirement for excavation.

Geotextiles in pavement construction are growing in popularity as this method has proven to be effective [28]. Geotextiles have different functions as those of separation / stabilization applications, reinforcement, and filtration, while they can be laid beneath both paved and unpaved roadways. They can be used in place of or in addition to natural aggregate building materials to address cost and environmental considerations [28]. Authors in [29] explored a wide range of stressors, involving those related to building highways. They found that the subgrade soil, which serves as the pavement foundation, has a significant impact on flexible pavement performance. Moreover, it is constant across a wide range of soil types and less susceptible to the environment. In this study, various combinations of non-woven geotextiles were employed. The Indian Standard Code (IS: 2720) was followed to conduct the tests for compaction, soaking CBR, and Unconfined Compressive Strength (UCS) [29]. On the other hand, geotextiles have some drawbacks as they can be affected by chemicals, moisture, and UV radiation. The fibers may degrade over time, decreasing the material functionality. Additionally, geotextiles are less load-bearing than conventional materials like concrete and gravel and might not be appropriate for uses where a large load-carrying capacity is needed. Therefore, it is crucial to choose a geotextile that is strong enough to resist the project site environmental factors and capable of withstanding the project load requirements [30, 31].

The aim of this research is to experimentally investigate the effect of EEC and geotextile materials on the mitigation of

reflective cracks. The experimental work included the utilization of ECC interlayers of thicknesses of 7, 12, and 17 mm as well as geotextile fabric positioning (at base and at 1/3 depth from the base of the asphalt concrete specimen).

II. MATERIALS AND METHODS

A. Engineered Cementitious Composite (ECC)

The raw materials selected to prepare the ECC mix for this research comprised Portland cement, silica fume, fine aggregates (sand) conforming to ASTM C33 gradation, tap water, and steel fibers. Cement and sand properties are shown in Table II and the properties of silica fume and steel fibers in Table III. The formulated mix design for this investigation is illustrated in Table IV. It predominantly uses materials that are readily available locally to reduce the production cost. Through preliminary testing, it was determined that this specific mix design yields an average compressive strength of about 50 MPa in 28 days as well as a modulus of rupture of 19 MPa. For the ECC preparation, the dry ingredients, excluding the steel fibers, were initially blended in a mechanical mixer for two minutes as per [32]. The steel fibers were then introduced and blended uniformly with the dry mix, see Figure 1. Following the even distribution of the fibers, water was systematically added and mixed for an additional 2 min. After achieving the appropriate consistency, ECC was cast into plate molds with dimensions of 375×75×25 mm, as in [32]. The samples were de-molded after 24 hr and cured in a water bath for 28 days at 20 ± 2 °C.

TABLE II. PROPERTIES OF CEMENT AND SAND

Cement									
Chemical composition %	CaO	SiO_2	Al_2O_3	Fe_2O_3	MgO	K_2O	SO_3	IR	L.O.I
Result	60.72	20.22	4.41	5.03	3.72	0.34	2.19	0.97	2.4
Physical properties	**Specific gravity**		**Fineness (m^2/kg)**	**Setting (min.)**		**Compressive strength (MPa)**			
				Initial	Final	3 days		7 days	
Result	3.17		326	110	270	21		34	
Sand									
Physical properties	**Specific gravity (bulk)**					**Absorption, %**			
Results	2.63					1.08			
Gradation, sieve size (mm)	9.5	4.75	2.36	1.18		0.6	0.3	0.15	
% passing	100	96	84	68		45	16	3	

TABLE III. PROPERTIES OF SILICA FUME AND STEEL FIBERS

Silica Fume			
Physical properties	Color	Specific gravity	Fineness (m^2/kg)
Results	Grey	2.27	Min15000
Steel fiber			
Physical properties	Average length (mm)	Average diameter (mm)	Density (kg/m^3)	Tensile strength (MPa)
Results	13	0.3	7864	2860

TABLE IV. MIX DESIGN OF ECC

Material	**Cement**	**Sand**	**Silica fume**	**Water**	**Steel fibers**
Content (kg/m^3)	900	1000	100	400	2% by volume

B. Asphalt Concrete

The raw materials selected to prepare the asphalt concrete mix for this research included the asphalt cement that was procured from the Doura oil refinery, situated in the southwestern part of Baghdad. The latter underwent tests based on the Superpave performance grade requirements (Figure 3). The results, detailed in Table V, verify that the asphalt cement aligns with the PG 64-16 grade requirements. The aggregate used for this experimental study was crushed quartz, sourced from the Amanat Baghdad asphalt concrete mix plant in the northern region of Baghdad. The aggregate coarse and fine fractions were separated utilizing sieves. They were later recombined in the right ratios to align with the grading criteria for a mix of wearing course type IIIA, depending on SCRB/R9 specification [33]. The aggregate physical properties are presented in Table VI. Figure 2 illustrates the aggregate gradation curve. The mineral filler employed is ordinary Portland cement, sourced from a cement factory in Kubaissa (west of Iraq), as shown in Table VII. In this study, Kevlar Aramid fiber was employed as a geotextile to strengthen asphalt concrete, as shown in Table VIII. The geotextile was cut into 400×300 mm strips, matching the size of the asphalt concrete slab samples. It was positioned in two specific locations: at the specimen base and at 1/3 depth from the base. To promote bonding between the geotextile and the asphalt concrete, and to maintain consistent asphalt cement in the mix, the geotextile strip was pre-coated with a liquid asphalt layer (tack coat) prior to its insertion into the specimen.

Fig. 1. Blending the ECC contents with a mechanical mixer.

TABLE V. ASPHALT CEMENT PROPERTIES

Asphalt cement	Properties	Designation	Measured temperature (°C)	Measured parameters	Specification requirements [34]
Original	Flash Point (°C)		-	292	230 °C, min
	Viscosity at 135 °C (Pa.s)	AASHTO T316	-	0.454	3 Pa.s, max
	DSR, G/sinδ at 10 rad/s (kPa)	AASHTO T315	58	3.3108	1.00 kPa, min
			64	2.1887	
			70	0.946	
RTFO Aged	Mass Loss (%)	AASHTO T240	-	0.708	1%, max
	DSR, G/sinδ at 10 rad/s (kPa)	AASHTO T315	58	4.0337	2.2 kPa, min
			64	3.1667	
			70	2.0774	
PAV Aged	DSR, G.sinδ at 10 rad/s (kPa)		28	4394	5000 kPa, max
			25	6371	
	BBR, Creep Stiffness (MPa)	AASHTO T313	-6	119.8	300 MPa, max

TABLE VI. AGGREGATE PHYSICAL PROPERTIES

Test	ASTM standard	Result	Specification requirements [33]
Coarse Aggregate			
Apparent specific gravity	C127	2.652	-
Bulk specific gravity		2.631	-
Water absorption (%)		0.287	-
Soundness (sodium sulfate solution loss) (%)	C88	3.5	12 max.
Wear percentage (Los Angeles abrasion) (%)	C131	18	30 max.
Flat and elongated (5:1) (%)	D4791	3	10 max.
Fractured pieces (%)	D5821	92	90 min.
Fine Aggregate			
Apparent specific gravity	C128	2.611	-
Bulk specific gravity		2.537	-
Water absorption (%)		0.902	-
Clay lump and friable particles (%)	C142	1.21	3 max.
Sand equivalent (%)	D2419	58	45 min.

TABLE VII. PHYSICAL PROPERTIES OF MINERAL FILLER

Test	Results
Specific gravity	3.17
Passing sieve No.200 (%)	98

TABLE VIII. PHYSICAL PROPERTIES OF GEOTEXTILE

Product Type	Aramid woven fabric
Style/Pattern	Unidirectional twill
Material	Phenylene terephthalamide polymer
Thickness	1 mm
Color	Yellow
Tensile strength (gpd)	24
Density (kg/m^3)	1451

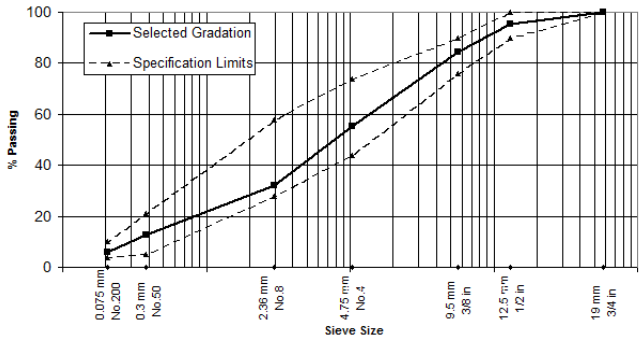

Fig. 2. Aggregate gradation curve for wearing course.

Fig. 3. Asphalt cement tests.

C. Asphalt Concrete Mix Design

The mix design for asphalt concrete specimens was carried out using the Marshall method [35]. Each specimen was prepared by compacting 75 blows on each side via an automatic Marshall compactor. The Optimum Asphalt Content (OAC) is determined as the average of the three asphalt content values that yield the highest stability, maximum density, and 4% air void content, as outlined in AI's manual series No. 2 [36].

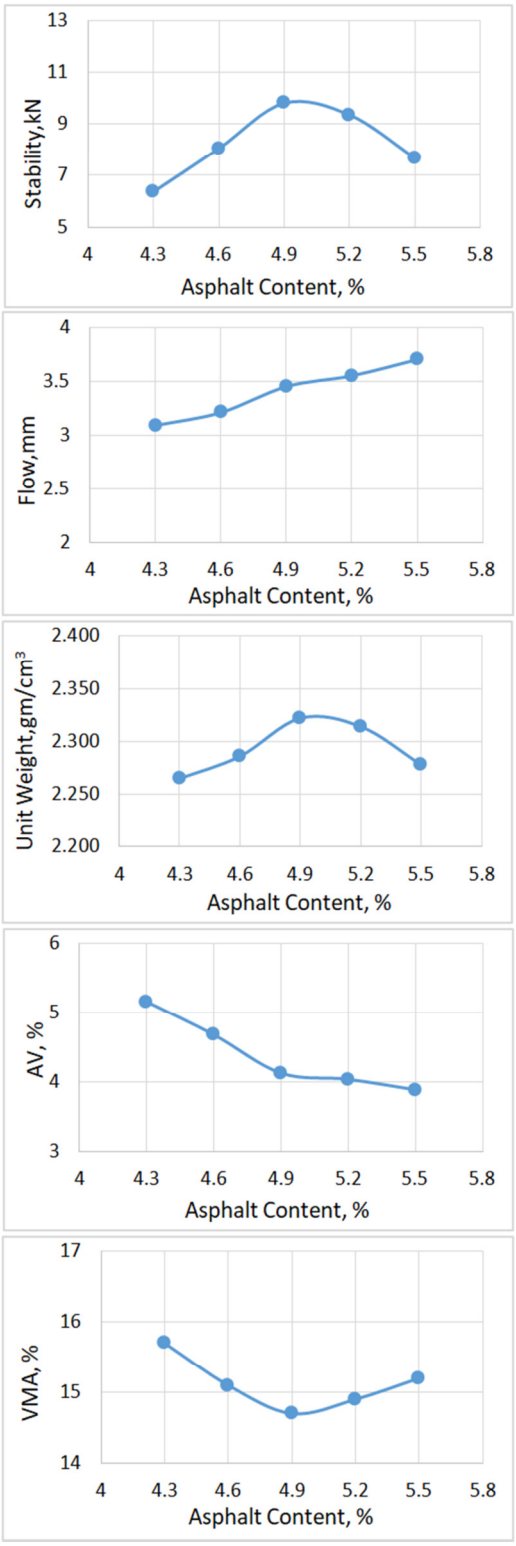

Fig. 4. Mix design results of asphalt concrete with the Marshall method.

Five different asphalt cement percentages were tried, starting at 4% by weight of the total mix and increased by 0.5 percent increments, resulting in tests at 4.0, 4.5, 5.0, 5.5, and 6%. Figure 4 presents the results for stability, flow, density, and volumetric properties, like AV% and VMA%. The optimal asphalt content was determined as 5.0% by weight of the total mix. At this content, both the flow value and VMA% met the set standards: 2 to 4 mm for flow and over 14% for VMA.

D. Preparation of Asphalt Concrete Mix

During the specimen preparation, the aggregate was separated using sieves of certain sizes: 19, 12.5, 9.5, 4.75, 2.36, 0.3, 0.075 mm and a pan as shown in Figure 1. The aggregate was combined in a preparation bowl and weighed based on the intended specimen shape and test type. The mixed aggregate was blended uniformly for two minutes and heated at 150 °C for 2 hr. The bowl was subsequently weighed and a predetermined quantity of asphalt cement, preheated to a range of 150–155 °C (aligning with a binder viscosity of 170 ± 20 c.St), was added in the mixture. The bowl content was thoroughly mixed on a hot plate for 2 min. To achieve a consistent compaction temperature, the bowl was then placed in an oven for 10 min at 140 °C. Meanwhile, the mold was pre-heated at 100 °C. The material was then transferred to the mold and compacted as per test specifications, using a Marshall compactor for cylindrical specimens and a roller compactor for slab specimens. The roller compaction was performed in five progressive phases with varying forces, ranging from 0.5 kN to 4 kN. Different loading cycles were applied in each phase. The compaction was ended once the sample density matched the predetermined Marshall density. For the Marshall Test, the sample weight was 1150 gm, while for the slab specimen, later trimmed for prisms for the OT test, the weight was 13340 gm. In the case where the geotextile was integrated at a depth of one-third from the specimen base, a two-phase compaction approach was implemented. At the beginning, a third of the total mix weight was introduced into the mold, undergoing the initial compaction phase with a force of 0.5 kN across 5 loading cycles. After this initial compaction, the geotextile was laid on top of the already compacted portion. The remaining two-thirds of the mix were then added to the mold and the compaction continued accordingly. Subsequently, the slab specimen was trimmed using a rock cutter to achieve the required dimensions of 375×75× 50 mm.

E. Overlay Test (OT) Procedure

The OT evaluates the susceptibility of asphalt mixtures to reflection cracking and explores the potential of ECC as an interlayer system as well as geotextile fabric in mitigating reflection cracking. In this test, each specimen type was replicated three times to ensure the accuracy and consistency of the results. In the case of the ECC interlayer usage, the asphalt concrete prism is bonded to the ECC prism with a dimension of 375×75 mm employing different heights of ECC: 7 mm, 12 mm, and 17 mm. When geotextile at the bottom of asphalt concrete prisms was used, the geotextile was tacked to the bottom of asphalt concrete prisms utilizing liquid asphalt (tack coat). For a more realistic field representation, the asphalt sample either strengthened or unstrengthened, is bonded to two Portland Cement Concrete (PCC) prisms, each 75 mm wide and 50 mm high, applying epoxy glue. These PCC prisms serve as a base, representing the concrete pavement beneath typical asphalt overlays in practical conditions. The complete setup

was then attached to two horizontal steel platforms of an overlay testing apparatus separated by a gap of 5 mm, which imitates the width of joints or cracks in actual overlaid roads. To facilitate optimal bonding, a sustained weight of 10 kg was positioned atop the asphalt concrete layer for 60 min. The sample setup is exhibited in Figure 5.

Conforming to ASTM WK26816 guidelines [37], the test was conducted under displacement control mode, utilizing one cycle every 10 s. The sliding platform moves in a cyclic triangular waveform, consistently reaching a maximum shift of 0.635 mm (0.025 inches) at a testing temperature of 20 °C. The key result of the OT is the number of load cycles to failure (Nf). Authors in [39] illustrated that failure is initiated when the peak load in a cycle decreases to 93% below the highest initial load [38, 40-42]. Another two parameters that can be extracted from this test are the critical fracture energy (Gc) and the Crack Progression Rate (CPR). Figure 6 displays the cycles of the implemented displacement, load, and their related time sequences. Furthermore, Figure 6 illustrates the variation in the peak tensile load as related to the number of loading cycles and the typical first hysteresis loop. Subsequently, Gc is calculated using the equation Gc=W/A, where W encapsulates the area under the load-tension curve (from zero load to maximum tension load) and A represents the specimen cross-sectional area (width × height). Gc represents the energy required to initiate a crack at the bottom plane of the specimen during the initial loading phase. A higher Gc suggests that the asphalt mix requires more energy to initiate the crack, indicating enhanced resistance to the onset of reflection cracking. In contrast, CPR demonstrates the specimen crack resistance during the propagation phase. It is derived from fitting a power equation to the curve that represents the decrease in load with the increasing number of loading cycles, where the power term b in the fitted equation is consistently negative. For practical considerations, the absolute value of b is termed as the CPR. A higher CPR denotes accelerated crack propagation within the asphalt specimen, which may result in a shorter lifespan for the asphalt concrete.

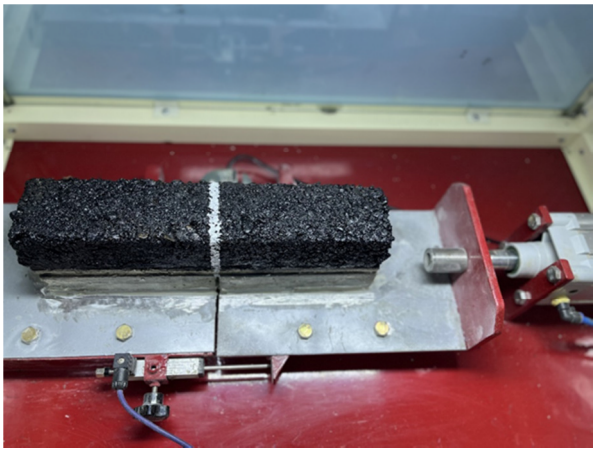

Fig. 5. Overlay test setup.

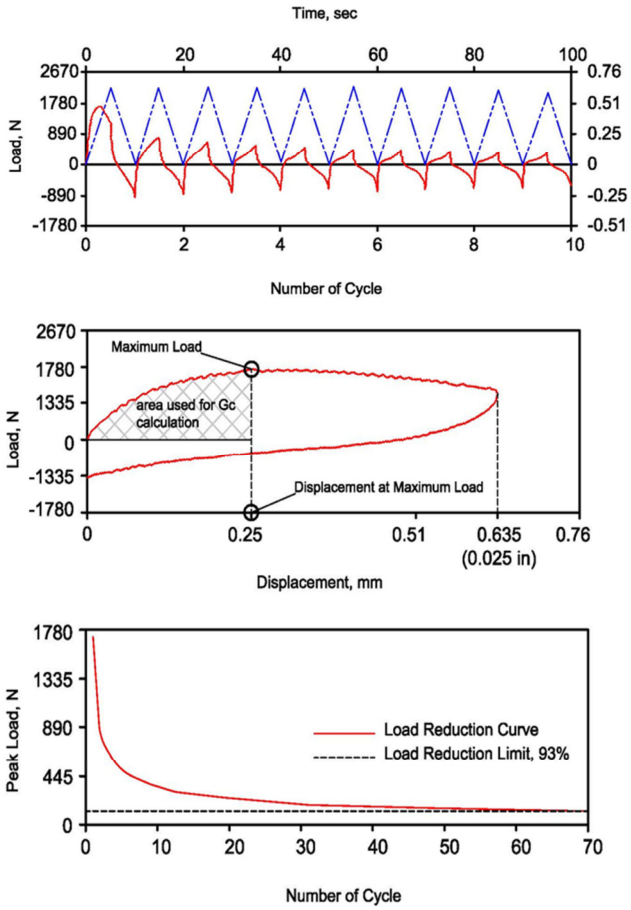

Fig. 6. Typical output for OT.

III. RESULTS AND DISCUSSION

A. *Effect of ECC on Reflection Cracking*

Figure 7(a) presents the discernible enhancement in the Gc values, a measure of the energy required to initiate a crack as the thickness of the ECC interlayer increases. When compared to the Reference Specimen (RS), which exhibits a Gc value of 0.5701 kJ/mm^2, there is a marked improvement in the ECC samples. The ECC7 displays an approximately 78% increase in Gc, while ECC12 and ECC17 manifest 185% and 269% boost, respectively. This amplification in Gc suggests that asphalt mixes integrated with thicker ECC interlayers show superior resistance to the reflection cracking inception, signifying their potential efficacy in infrastructure longevity. Concurrently, the declining trend in CPR values, evidenced in Figure 7(b), confirms that once a crack is formed, its spread is remarkably slower in ECC-integrated specimens as opposed to the RS. Starting with the RS, a CPR of 0.361 is observed, setting a benchmark for subsequent evaluations. With the introduction of ECC7, the CPR sharply drops to 0.174, marking an approximate 52% reduction. The trend of diminishing CPR continues with ECC12, registering a value of 0.132, which translates to a further decrease of around 24% compared to ECC7. The peak of resistance is achieved with the ECC17 mix, which has the lowest CPR of 0.081. This value designates a reduction of nearly 78% compared to the RS.

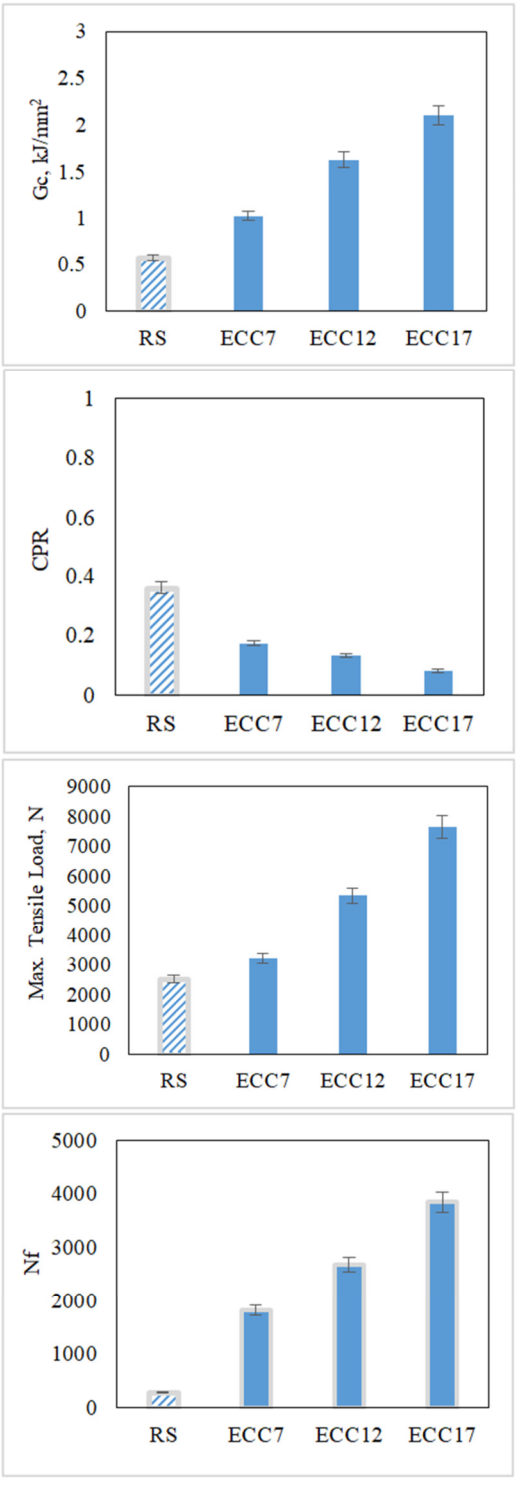

Fig. 7. Effect of ECC on different reflection cracking parameters. (a) Gc, (b) CPR, (c) max tensile load, (d) Nf.

With differing ECC interlayer thicknesses, Figure 7(c) provides a clear visual representation of the maximum tensile load capacities of various asphalt mixes. The maximum tensile load is a critical parameter as it determines the ultimate force a material can withstand before significant deformation or failure occurs, indicating the material toughness. In examining the RS, it displays a tensile load capacity of 2528.4 N. Introducing ECC into the mix exhibits a notable increase in this capacity. The ECC7, for instance, holds a load of 3230 N, marking an increase of about 27.8% relative to the RS. A thicker ECC interlayer, ECC 12, shows an even higher load capacity, resulting in a maximum load of 5345 N corresponding to an improvement of 111.5% compared to the RS. The peak load is reached with ECC17, which sustains a staggering load of 7638 N resulting in a gain of over 202% compared to the reference specimen RS. The presented trend suggests that the incorporation of thicker ECC interlayers substantially amplifies the tensile strength of the asphalt concrete overlay. This enhancement is paramount for overlayed pavement that endures daily mechanical stresses, emphasizing ECC's potential to reduce the likelihood of early damage.

The results of Nf, as presented in Figure7(d), agree with those obtained from the other reflection cracking parameters, showcasing a consistent pattern of performance enhancement. Significant improvements are visible with the use of ECC interlayers when compared to the RS, with an Nf value of 294. The ECC7 registers an Nf value of 1824, marking a noticeable improvement of approximately 520% compared to RS. ECC12 showcases an Nf of 2674, equating to an enhancement of around 810% over the RS. This upward trend peaks with ECC17, which commands an Nf value of 3845, signaling an extraordinary enhancement of roughly 1307% in relation to the RS.

Based on the data presented, it is evident that the use of ECC interlayers substantially ameliorates resistance to reflection cracking. The progressive improvements observed across varying ECC thicknesses highlight its pivotal role in ensuring superior performance and durability in pavement overlay applications

B. Effect of Geotextile on Reflection Cracking

Reviewing the Gc values presented in Figure 8(a), a clear enhancement is observed with the geotextile incorporation. The RS specimen displays a baseline Gc value of 0.5701 kJ/mm^2. When the geotextile is placed at the bottom (GB), the Gc value shows an increase to 0.8305 kJ/mm^2, marking a 45.7% improvement. Positioning the geotextile at 1/3 depth from the bottom (G1/3) yields a Gc value of 0.9821 kJ/mm^2, denoting a 72.3% enhancement from the RS. This suggests that geotextile placement, particularly at 1/3 depth, can contribute significantly to the energy required to initiate the crack. For the CPR outcomes, the RS stands at 0.361. However, with the GB incorporation, a slight reduction to 0.321 is observed, translated to an 11.1% improvement. A more pronounced decrease is evident with G1/3, which displays a CPR of 0.194, representing a 46.3% improvement. Such figures indicate the reduced crack propagation risk with geotextile placement, especially at 1/3 depth, as shown in Figure 8(b).

When considering the maximum tensile load a specimen can endure, it is imperative to note the inherent potential and improvements associated with the use of geotextile materials. As shown in Figure 8(c), the RS yields a maximum tensile load of about 2528.4 N.

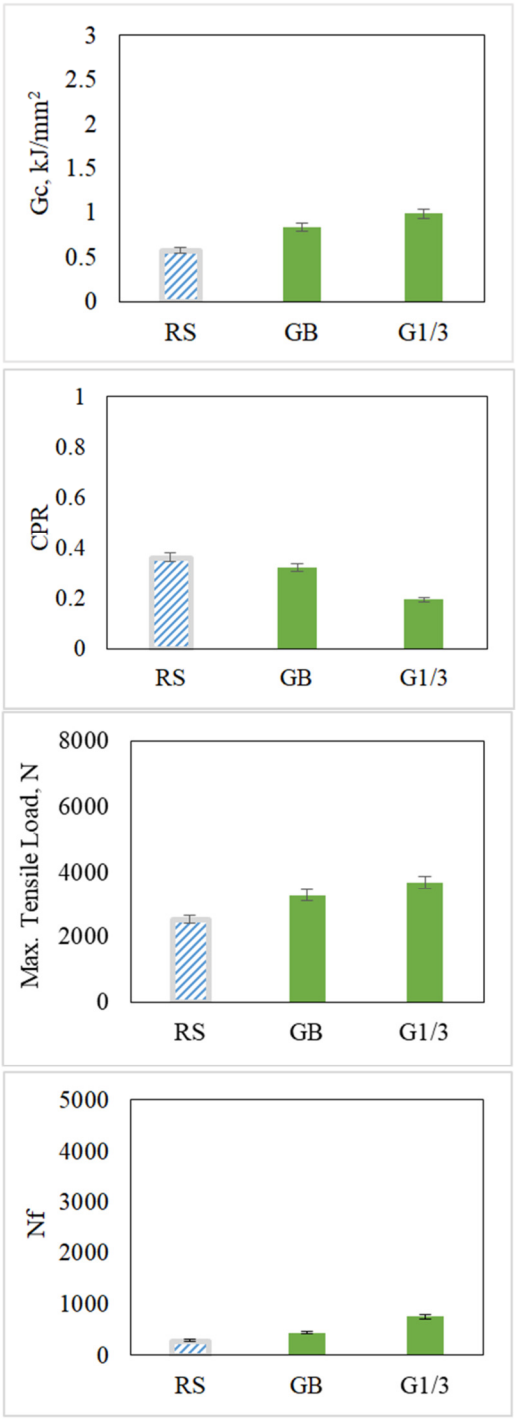

Fig. 8. Effect of geotextile on different reflection cracking parameters. (a) Gc, (b) CPR, (c) max tensile load, (d) Nf.

Introducing geotextile at the bottom (GB) brings forth a transformative change. The load measurement surges to 3273.2 N, marking an increase of 744.8 N, i.e. an appreciable 29.5% improvement in comparison with the RS. This increment is indicative of the added tensile strength and robustness incorporated due to the geotextile placement at the base. However, shifting the geotextile to 1/3 depth from the bottom (G1/3) advances the tensile load even further. This results in a maximum load of 3675 N, an increase of 146.8 N from GB and a substantial 1146.6 N leap from RS. This difference places the G1/3 improvement at a significant 45.4% over the RS. Not only does such a figure emphasize the structural fortification provided by geotextile, but also underlines the noticeable advantage of its placement at 1/3 depth.

The results regarding the Nf parameter are exhibited in Figure 8(d). The RS establishes the baseline with an Nf value of 294. This fundamental figure offers a perspective on the endurance and lifespan of a typical specimen when subjected to repeated stresses. With GB incorporation, the Nf shows a discernible increase, reaching an Nf of 445. This elevation, accounting for 151 from the RS, signifies a commendable 51.4% enhancement. The trend of improvement rises with the G1/3. The Nf ascends to 754, marking a spike of 309 from GB and a substantial 460 from the base RS. This denotes an outstanding 156.5% amplification over the RS. Such pronounced increments underscore the extended service life and reinforced resilience against cyclical loadings offered by geotextiles, especially when located at 1/3 depth.

As a result, the findings obtained highlight the pivotal role that geotextile installation plays in enhancing the ability of asphalt specimens to resist reflection cracking. The consistent outperformance of the G1/3 configuration accentuates the potential benefits of geotextile positioning in extending infrastructure durability and lifespan.

C. Performance Comparison of ECC and Geotextile

Figure 9 shows the performance related to reflection cracking of specimens strengthened using an ECC interlayer of varied thicknesses compared with those reinforced with geotextile at different positions. This Figure also presents the key parameters including Gc, CPR, maximum tensile load at the first loading cycle, and Nf.

The results shown in Figure 9(a) clearly illustrate that overlays reinforced with ECC, particularly ECC17, typically exhibit higher average Gc values when compared to the reference specimen and overlays reinforced with geotextile. This is indicative of their augmented ability to resist fracture, suggesting they can endure more stress before the onset of cracking. The improvement rate in the Gc value for ECC17 was found to be 153%, 96%, and 22% in relation to GB, ECC12, and ECC7 specimens, respectively. Based on [39], a Gc threshold of 0.5 differentiates a soft mix (below 0.5 N.mm/mm^2) and a tough mix (0.5 N.mm/mm^2 or more). The mixes with high toughness offer excellent resistance to the onset of reflection cracking. Based on Figure 9(a), the ECC specimens generally perform better than those with geotextiles. Furthermore, specimens reinforced with geotextile at 1/3 the depth from the bottom of the asphalt concrete specimen perform better than those with geotextile at the bottom.

Specimens ECC12 and ECC17 notably exhibit lower CPR values. This suggests a slower rate of crack development compared to the GB and G1/3 specimens. The inherent characteristics of ECC likely contribute to this behavior, offering increased resistance to crack progression, thereby potentially extending the asphalt overlay service life. In a direct

comparison with the GB and G1/3 specimens, ECC17 exhibited a CPR reduction of 75%, while ECC12 showed a 59% reduction. Using the criteria set in [39], where a CPR value of 0.5 differentiates between materials resistant to cracking (≤ 0.5) and those more vulnerable (> 0.5), mixes strengthened by ECC clearly outperform GB and G1/3, while G1/3 demonstrates better crack resistance than GB.

(a)

(b)

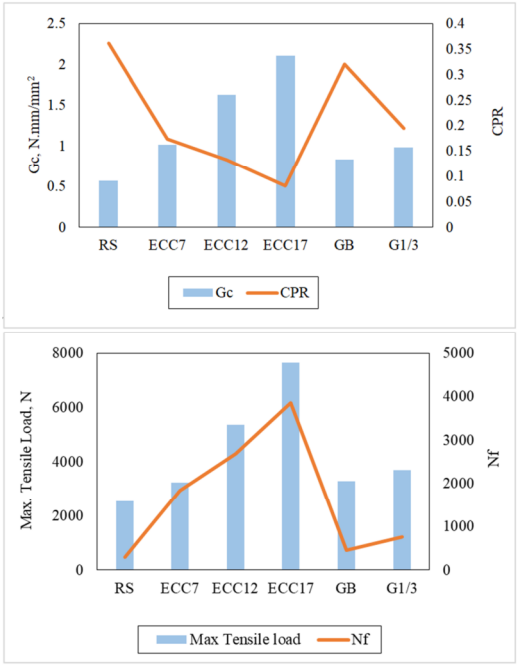

Fig. 9. The parameters for reflection cracking for ECC and Geotextile specimens. (a) Fracture energy (Gc) and crack progation rate (CPR), (b) maximum tensile load and Nf.

According to the maximum tensile load values shown in Figure 9(b), a clear trend emerges when examining the impact of ECC reinforcement. ECC12 yields an impressive increase of 63% in the maximum tensile load, emphasizing its notable capability to withstand tension during the initial loading cycle. Meanwhile, ECC17 stands out with a remarkable enhancement of 134% in tensile strength. This underscores the essential role that the amount of ECC plays in augmenting the overlay tensile resilience. Among the variants, ECC17 is the clear standout. Conversely, ECC7 demonstrates only a marginal improvement when compared to the reference specimen. In the context of the GB and G1/3 specimens, GB displays a slightly better tensile performance than G1/3.

The number of load cycles to failure (Nf) for different mix types exhibited in Figure 9(b), underscores the superior performance of ECC-strength mixtures when contrasted with the specimen reinforced with GB. ECC7 showcases a significant improvement, presenting an increase of approximately 310% over GB. This enhancement becomes even more pronounced with ECC12, which offers a growth of about 501%. The peak performance is reached with ECC17, marking a staggering rise of roughly 764% compared to GB. In the geotextile category, while G1/3 surpasses GB with a growth of approximately 69%, it does not come close to the performance metrics set by the ECC mixtures. In summary, ECC variants, especially ECC17, illustrate a decisive advantage in reflection cracking resistance over GB, and although G1/3 is superior to GB, it lags significantly behind the ECC mixtures in terms of percentage increase for Nf.

IV. CONCLUSIONS AND RECOMMENDATIONS

Based on the test results obtained in this study, the following conclusions can be drawn:

- Overlays strengthened with ECC, particularly ECC17, display a higher resistance to reflection cracking compared to the reference specimen (RS). Their higher average Gc values indicate a better ability to resist fracture compared to both RS and specimens reinforced with geotextile.
- In comparison to the RS, ECC specimens in general fare better against reflection cracking. Within the geotextile placements, specimens positioned at 1/3 depth from the bottom outperformed those placed directly at the bottom.
- Crack Propagation Rate (CPR) findings revealed that ECC12 and ECC17 possess a superior capacity to decelerate crack development. Specifically, ECC17 recorded a 75% reduction, and ECC12 reported a 59% reduction in CPR, distinguishing them as more resilient than the GB and G1/3 specimens.
- In the context of tensile strength, ECC17 exhibited a 134% augmentation, underscoring the pivotal role of ECC in boosting tensile resilience in overlays. On the contrary, ECC7 showed a marginal enhancement compared to the RS.
- ECC mixtures, with ECC17 in particular, demonstrated a pronounced advantage in the number of load cycles to failure (Nf) over the GB specimen. With ECC17 recording a significant surge of roughly 764% compared to GB, its dominance is evident.
- Although the G1/3 variant reinforced with geotextile surpassed the GB in performance parameters, it notably trailed the ECC-enhanced mixtures, especially when considering the percentage surge for Nf. The Nf for the average of ECC specimens is larger than the average Nf of the geotextiles specimens by 463 %.

Since the results are limited to the available materials and testing programs, future research is recommended to explore cost optimization strategies for different ECC thicknesses. Additionally, considering alternative fibers in ECC mixes is advised. It is essential to validate the experimental findings using field-based trial sections.

REFERENCES

[1] J. Baek, *Modeling reflective cracking development in hot-mix asphalt overlays and quantification of control techniques*. Ann Arbor, MI, USA: ProQuest LLC, 2010.

[2] J. Pais, "The Reflective Cracking in Flexible Pavements," *Romanian Journal of Transport Infrastructure*, vol. 2, no. 1, pp. 63–87, Jul. 2013, https://doi.org/10.1515/rjti-2015-0012.

[3] A. H. Albayati, Y. S. Ajool, and A. A. Allawi, "Comparative Analysis of Reinforced Asphalt Concrete Overlays: Effects of Thickness and Temperature," *Materials*, vol. 16, no. 17, Jan. 2023, Art. no. 5990, https://doi.org/10.3390/ma16175990.

[4] H.-J. Chen and D. A. Frederick, "Interlayers on Flexible Pavements (Abridgment)," *Transportation Research Record*, no. 1374, pp. 90–94, 1992.

[5] N. Dhakal, M. A. Elseifi, and Z. Zhang, "Mitigation strategies for reflection cracking in rehabilitated pavements – A synthesis," *International Journal of Pavement Research and Technology*, vol. 9, no. 3, pp. 228–239, May 2016, https://doi.org/10.1016/j.ijprt.2016.05.001.

[6] C. Gurp and A. A. A. Molenaar, "Simplified Method to Predict Reflective Cracking in Asphalt Overlays," in *Reflective Cracking in Pavements*, Liege, Belgium: CEP-LMP State University of Liege, 1989, pp. 190–198.

[7] P. Su and M. Li, "Review of Reflection Cracking Preventive Technologies on Asphalt Pavement with Semi-Rigid Base Course," *Journal of Physics: Conference Series*, vol. 1549, no. 3, Mar. 2020, Art. no. 032108, https://doi.org/10.1088/1742-6596/1549/3/032108.

[8] *Design & Maintenance Guide 33: Reflection cracking on airfield pavements – A design guide for assessment, treatment selection and future minimisation*, 1st ed. UK: Crown, 2005.

[9] M. Elseifi and R. Bandaru, "Cost effective prevention of reflective cracking of composite pavement.," Louisiana State University, Baton Rouge, LA, USA, FHWA/LA.11/478, Sep. 2011.

[10] M. J. Marquart, *Evaluation of Saw and Seal over the Overlaid Existing Concrete Joints*, vol. 94. North Dakota Department of Transportation, Materials and Research Division., 2001.

[11] D. A. Carroll, R. Cheng, R. J. Eger, L. Grusczynski, J. Marlowe, and H. H. Titi, "Implementing Highway Preventive Maintenance: Comparing Challenges, Processes, and Solutions in Three States," *Transportation Research Record*, vol. 1877, no. 1, pp. 10–16, Jan. 2004, https://doi.org/10.3141/1877-02.

[12] D. Timm and A. Warren, "Performance of Rubblized Pavement Sections in Alabama," Final Report, Oct. 2011.

[13] H. Ceylan, K. Gopalakrishnan, and S. Kim, "Rehabilitation of Concrete Pavements Utilizing Rubblization," Center for Transportation Research and Education, Ames, IA, USA, IHRB Project TR-550; CTRE Project 05-237, Apr. 2008.

[14] S. J. Ellis, P. C. Langdale, and J. Cook, "Performance of Techniques to Minimize Reflection Cracking and Associated Developments in Pavement Investigation for Maintenance of UK Military Airfield," presented at the 2002 Federal Aviation Administration Airport Technology Transfer Conference, Crowthorne, UK, May 2002.

[15] J. W. Button and R. L. Lytton, "Guidelines for Using Geosynthetics with Hot-Mix Asphalt Overlays to Reduce Reflective Cracking," *Transportation Research Record*, vol. 2004, no. 1, pp. 111–119, Jan. 2007, https://doi.org/10.3141/2004-12.

[16] S. Fallah and A. Khodaii, "Evaluation of parameters affecting reflection cracking in geogrid-reinforced overlay," *Journal of Central South University*, vol. 22, no. 3, pp. 1016–1025, Mar. 2015, https://doi.org/10.1007/s11771-015-2612-9.

[17] S. Deilami and G. White, "Review of reflective cracking in composite pavements," *International Journal of Pavement Research and Technology*, vol. 13, no. 5, pp. 524–535, Sep. 2020, https://doi.org/10.1007/s42947-020-0332-5.

[18] M. Bhuyan, M. Khattak, Q. Zhang, and E. Schlader, "Experimental Evaluation of Engineered Cementitious Composites as Reflective Crack Control Interlayer for Composite Pavements," *MATEC Web of Conferences*, vol. 271, 2019, Art. no. 07002, https://doi.org/10.1051/matecconf/201927107002.

[19] M. Luo, "Mechanical analysis of asphalt stabilized permeable base to inhibit reflective cracking," *IOP Conference Series: Materials Science and Engineering*, vol. 231, no. 1, Jun. 2017, Art. no. 012090, https://doi.org/10.1088/1757-899X/231/1/012090.

[20] Y.-Q. Tan, K.-L. Shi, L.-M. Li, G.-M. Chen, and L. Ji, "Prevention of reflective cracks with high viscous asphalt stress absorbing layer," *Journal of Harbin Institute of Technology*, vol. 40, no. 2, pp. 241–245, Feb. 2008.

[21] H. Ceylan, K. Gopalakrishnan, and R. L. Lytton, "Neural Networks Modeling of Stress Growth in Asphalt Overlays due to Load and Thermal Effects during Reflection Cracking," *Journal of Materials in Civil Engineering*, vol. 23, no. 3, pp. 221–229, Mar. 2011, https://doi.org/10.1061/(ASCE)MT.1943-5533.0000153.

[22] K. Madhavi, M. Venugopal, V. Rajesh, and K. Suresh, "Experimental Study on Bendable Concrete," *International Journal of Engineering Research and Technology*, vol. 5, no. 10, pp. 501–504, Oct. 2016, https://doi.org/10.17577/IJERTV5IS100400.

[23] Q. Zhang and M. Khattak, "Mitigating Reflective Cracking Through the Use of a Ductile Concrete Interlayer," University of Louisiana at Lafayette, Lafayette, LA, USA, 18PLSU13, Sep. 2019.

[24] S. Gadhiya, T. N. Patel, and D. Shah, "Bendable concrete: A review," *International Journal of Civil and Structural Engineering Research*, vol. 4, no. 1, pp. 141–147, 2015.

[25] M. Singh, B. Saini, and H. D. Chalak, "Properties of Engineered Cementitious Composites: A Review," in *1st International Conference on Sustainable Waste Management through Design*, Ludhiana, India, Nov. 2018, pp. 473–483, https://doi.org/10.1007/978-3-030-02707-0_54.

[26] T. Manzoor and S. Singh, "Impact Of Geotextile On Thickness Of Road Layers," *International Journal of Engineering Technology and Management Sciences*, vol. 5, no. 6, pp. 183–187, Sep. 2022, https://doi.org/10.46647/ijetms.2022.v06i05.026.

[27] P. Ahlawat, M. Pardeep, and V. Sharma, "A Review Paper On Geosynthetics In Road Construction," *International Journal of Progressive Research in Engineering Management and Science*, vol. 3, no. 4, pp. 80–85, 2023.

[28] H. Alimohammadi, "Effectiveness of Geogrids in Roadway Construction: Determine a Granular Equivalent (G.E.) Factor," Ph.D. dissertation, Iowa State University, Ames, IA, USA, 2021.

[29] A. Mittal, "Effect of Non-Woven Geotextile and Biaxial Geogrid Reinforcement on the Strength Behaviour of Subgrade Soil," *International Journal of Civil Engineering*, vol. 5, no. 10, pp. 28–32, Oct. 2018, https://doi.org/10.14445/23488352/IJCE-V5I10P105.

[30] M. Zvonaric and S. Dimter, "Prevention and remediation measures for reflective cracks in flexible pavements," *Gradevinar*, vol. 74, no. 03., pp. 189–197, Apr. 2022, https://doi.org/10.14256/JCE.3427.2021.

[31] H. Wu *et al.*, "Review of Application and Innovation of Geotextiles in Geotechnical Engineering," *Materials*, vol. 13, no. 7, Jan. 2020, Art. no. 1774, https://doi.org/10.3390/ma13071774.

[32] I. F. Al-Mulla, A. S. Al-Rihimy, and M. S. A. Alameer, "Properties of engineered cementitious composite concrete (bendable concrete) produced using Portland limestone cement," *IOP Conference Series: Materials Science and Engineering*, vol. 671, no. 1, Jan. 2020, Art. no. 012131, https://doi.org/10.1088/1757-899X/671/1/012131.

[33] *SCRB/R9. General Specification for Roads and Bridges, Section R/9, Hot-Mix Asphalt Concrete Pavement, Revised Edition*. Baghdad, Iraq: State Corporation of Roads and Bridges, Ministry of Housing and Construction, 2003.

[34] *AASHTO M 320: Standard Specification for Performance-Graded Asphalt Binder*. AASHTO, 2023.

[35] *ASTM D6927-22(2022), Standard Test Method for Marshall Stability and Flow of Asphalt Mixtures*. West Conshohocken, PA, USA: ASTM International, 2022.

[36] *Performance Graded Asphalt Binder Specification and Testing*. Lexington, KY, USA: Asphalt Institute, 1981.

[37] *ASTM WK87316-09(2009), New Test Methods for Determining the Susceptibility of Asphalt Mixtures to Cracking Using the Overlay Tester*. West Conshohocken, PA, USA: ASTM International, 2009.

[38] F. Zhou, S. Hu, and T. Scullion, "Integrated asphalt (overlay) mixture design, balancing rutting and cracking requirements," Texas Transportation Institute, Austin, TX, USA, Technical Report FHWA/TX-06/0-5123-1, 2005.

[39] H. Sadek, M. Hassan, C. Berryman, M. Hossain, and I. Idris, "Evaluation of Asphalt Mixtures' Resistance to Cement-Treated Base

(CTB) Reflective Cracking in the Laboratory," Louisiana State University, Baton Rouge, LA, USA, Project No. 19BLSU02, Nov. 2020.

[40] S. S. Almasoudi and A. H. K. Albayati, "Statistical Analysis of Component Deviation from Job Mix Formula in Hot Mix Asphalt," *Engineering, Technology & Applied Science Research*, vol. 12, no. 5, pp. 9295–9301, Oct. 2022, https://doi.org/10.48084/etasr.5225.

[41] H. M. A. A. Kareem and A. H. K. Albayati, "The Possibility of Minimizing Rutting Distress in Asphalt Concrete Wearing Course," *Engineering, Technology & Applied Science Research*, vol. 12, no. 1, pp. 8063–8074, Feb. 2022, https://doi.org/10.48084/etasr.4669.

[42] F. Alzaidy and A. H. K. Albayati, "A Comparison between Static and Repeated Load Test to Predict Asphalt Concrete Rut Depth," *Engineering, Technology & Applied Science Research*, vol. 11, no. 4, pp. 7363–7369, Aug. 2021, https://doi.org/10.48084/etasr.4236.